

Compact Flat-Box Adsorbers for Air Separation by PSA Processes

Cheng-tung Chou, Chih-Feng Cheng, and Wei-Tzung Chen

Department of Chemical and Materials Engineering, National Central University, Chung-Li 32001, Taiwan (R.O.C.)

Abstract

Cylindrical adsorbers are usually used for pressure swing adsorption (PSA) processes. In this study, the flat-box adsorbers which stack together replaced the traditional cylindrical adsorbers. Simulation was performed for separation of air (21% oxygen; 79% nitrogen) in Skarstrom cycle. Instantaneous equilibrium between solid and gas phase with non-isothermal operation were assumed and the bed pressure drop could be neglected. The adsorption isotherms used were extended Langmuir isotherms and 5A zeolite was utilized as adsorbent. In addition, to verify the applicability of the simulation program on the system of air separation with 5A zeolite, the simulation results of the cylindrical adsorbers were compared with the experimental data in literature. The simulation results were in good agreement with experimental data obtained elsewhere, and showed the reliability of this PSA simulation program. The simulation results of flat-box adsorbers and traditional cylindrical adsorbers were compared. The performance of the flat-box adsorbers was similar to that of the traditional cylindrical adsorbers when the heat transfer coefficient between neighboring adsorbers is set at $14.049 \text{ J/K}\cdot\text{m}^2\cdot\text{s}$ at same purge to feed ratio and product to feed ratio. But the flat-box adsorbers were better than the cylindrical adsorbers in the usage of packing space. The effects of operating variables such as step time, bed length, adsorption pressure, the heat transfer coefficient between neighboring adsorbers were investigated on the performance of PSA.

Keyword: pressure swing adsorption (PSA); flat-box adsorber; air separation

1. Introduction

Pressure swing adsorption (PSA) is a cyclic process for separation of gas mixtures. This Process used variation of pressures as the main operating parameter to achieve separation. In a PSA process, when the high pressure feed enters the adsorber from the feed end, adsorption occurs and the product of enriched weakly adsorbed component is obtained at the other end of the adsorber. This separation technology

needs lower energy and is less costly than the conventional separation processes like absorption and distillation. Since the early work of Skarstrom¹, pressure swing adsorption processes have found widespread and increasing applications in purification and bulk separation of gas mixtures.

In the previous study of Zhou et al.(2006), a new compact design of PSA has been employed. All columns of the PSA process were reduced to disks that were stacked together. The feasibility and performance of this new design were tested with a four-bed process experiment. However in their experiments, only experiments with stacked-disk adsorbers were performed. No comparison between stacked-disk adsorbers and conventional packed-bed adsorbers were made. In our study, PSA simulations are performed to compare the performance between new compact flat-box adsorbers and conventional packed-bed adsorbers. The PSA process for producing oxygen from air by utilizing 5A zeolite as adsorbent is studied.

2. Process Description

The new design of compact flat-box adsorbers which are stacked together are expected to reach higher performance of PSA by letting the released heat from the adsorption bed be transferred to the desorption bed. The Skarstrom cycle is chosen as case study, because when one bed is operating on adsorption step, the neighboring bed is operating on desorption step, which is suitable for the design of flat-box adsorbers PSA. The four steps of Skarstrom cycle schematic diagram are shown in Figure 1. The first step is (1) pressurization step, followed by (2) production step, (3) depressurization step, and (4) purge step.

The flat-box adsorber diagram is shown in Figure 2. Under the condition of the same cross sectional area as conventional packed-bed adsorber, the bed height to the bed width of flat-box adsorbers ratio is set 5.

Other parameters needed in simulation are showed in Tables 1-3.

3. Mathematical Model

This study is explored by simulation. Some assumptions in the theoretical model are shown below:

1. Local equilibrium model is used because simultaneous equilibrium between gas phase and solid phase is assumed.
2. The equilibrium relations for both oxygen and nitrogen on zeolite 5A are represented by extended Langmuir isotherm.
3. The ideal gas law is applicable.

4. The operating condition is non-isothermal.
5. Only concentration and temperature gradient in flowing direction are concerned.
6. The pressure drop is negligible.

Subject to these assumptions, the following set of equations describes the system:

Overall mass balance,

$$-\frac{\partial q}{\partial z} = \frac{\varepsilon A}{R} \frac{\partial (P/T)}{\partial t} + (1-\varepsilon)A \sum_{i=1}^n \frac{\partial n_i}{\partial t} \quad (1)$$

Mass balance for component i,

$$\frac{\partial}{\partial z} \left(\frac{\varepsilon A D_{ax,i} P}{RT} \frac{\partial y_i}{\partial z} \right) - \frac{\partial (y_i q)}{\partial z} = \frac{\varepsilon A}{R} \frac{\partial}{\partial t} \left(\frac{y_i P}{T} \right) + (1-\varepsilon)A \frac{\partial n_i}{\partial t} \quad (2)$$

where $i = 1, 2$

Energy balance for the traditional cylindrical adsorbers:

$$\begin{aligned} & (Ak) \frac{\partial^2 T}{\partial z^2} - \frac{\partial}{\partial z} (\bar{C}_p q T) - \pi D h (T - T_\infty) \\ & = \frac{\varepsilon A}{R} \frac{\partial}{\partial t} (\bar{C}_p P) + (1-\varepsilon)A \sum_{i=1}^n \frac{\partial}{\partial t} [n_i (\tilde{C}_{pi} T - H_i)] + (1-\varepsilon) \rho_s \hat{C}_{ps} A \frac{\partial T}{\partial t} \end{aligned} \quad (3)$$

Energy balance for the flax-box adsorbers:

$$\begin{aligned} & (Ak) \frac{\partial^2 T}{\partial z^2} - \frac{\partial}{\partial z} (\bar{C}_p q T) - (2b_h + b_w) h (T - T_\infty) - b_w h' (T - T_A) \\ & = \frac{\varepsilon A}{R} \frac{\partial}{\partial t} (\bar{C}_p P) + (1-\varepsilon)A \sum_{i=1}^n \frac{\partial}{\partial t} [n_i (\tilde{C}_{pi} T - H_i)] + (1-\varepsilon) \rho_s \hat{C}_{ps} A \frac{\partial T}{\partial t} \end{aligned} \quad (4)$$

From the extended Langmuir isotherm the equilibrium adsorption concentrations could be calculated as

$$n_i^* = \frac{\rho_s a_i y_i P}{1 + \sum_{j=1}^n b_j y_j P} \quad (5)$$

$$a_i = A_i \exp\left(\frac{H_i}{RT}\right), \quad b_i = B_i \exp\left(\frac{H_i}{RT}\right)$$

where n_i^* is equilibrium adsorptive amount

Axial dispersion coefficient is calculated by:

$$D_{ax,i} = \gamma D_{m,i} + \frac{0.5 \bar{u} d_p}{1 + \beta (D_{m,i} / \bar{u} d_p)} \quad (6)$$

$$\gamma \cong 0.75, \beta \cong 9.5, \bar{u} = \frac{u_0}{\varepsilon} = \frac{RT}{\varepsilon AP}, q = \frac{\theta}{\phi} QL$$

Within this simulation program, flow stream are built through the manipulated valves and the valve equation is used to calculate the transient flow rates at the both ends of beds in the theoretical calculation unless otherwise specified. the flow formula for gases recommended by Fluid Controls Institute Inc. was the valve equation used to calculate the flow rates at both ends of a bed:

$$Q^* = 77.01 c_v \left[\frac{P_1^2 - P_2^2}{SG \times T} \right]^{1/2} \quad \text{for } P_2 > 0.53P_1 \quad (9)$$

$$Q^* = 65.31 c_v P_1 \left[\frac{1}{SG \times T} \right]^{1/2} \quad \text{for } P_2 \leq 0.53P_1 \quad (10)$$

Where Q^* is flow rate in liter/min (1atm, 273K), P_1 is upstream pressure and P_2 represented downstream pressure.

Boundary conditions were assumed as follows:

For the inlet end:

$$c(t, 0) = c_{in}(t), T(t, 0) = T_{in}(t) \quad (7)$$

For the outlet end:

$$\frac{\partial c(t, L)}{\partial z} = 0, \frac{\partial T(t, L)}{\partial z} = 0 \quad (8)$$

When the simulation program begins to run, several basic grid points are marked in the bed and set up initial some initial value (like concentration, temperature, and pressure) at those points. The PDEs (partial differential equations) are converted to a set of ODEs (ordinary differential equations) with respect to time by the method of lines. The spatial derivatives of concentration, and gas temperature at every basic grid point are evaluated by upwind difference, and flow rates in the adsorbers are estimated by cubic spline approximation. The integration of concentration, temperature, and pressure with respect to time in the bed is done by the program LSODE from the package of ODEPACK. The simulation is stopped when the system reaches cyclic steady state. The details of calculation method are showed in Chou and Huang(1994) and Huang et al.(2006)

4. Results and Discussion

Comparison with Experimental Data

For confirming the accuracy of the theoretical model, the simulation program is verified by comparison with experimental results of Farooq et al.(1989). The definitions of recovery, purge to feed ratio, and product to feed ratio are described as following:

$$\text{Recovery} = \frac{\text{amount of oxygen in product}}{\text{amount of oxygen in feed}}$$

$$\text{Purge to Feed Ratio} = \frac{\text{amount of purge}}{\text{amount of feed}}$$

$$\text{Product to Feed Ratio} = \frac{\text{amount of product}}{\text{amount of feed}}$$

The comparison result between experiments and simulation is showed in Table 4. For comparing with experimental data, the calculated feed flow rate and product flow rate were adjusted to be close to the experimental results. The simulation results gave good agreements with the experimental data in purity and recovery. Figure 2 shows the change of pressure of both adsorbers with time. As observed from Figure 3, the bed temperature fluctuates between 287K and 316K. The maximum temperature different between two bed is above 18 K. Figures 4-7 show the purity of O₂ profile in four step. In the pressurization step, because the feed stream inputs to the bottom of bed, the concentration front moves from the bottom of bed to the top of bed. When the pressure reaches the setting of the adsorption pressure, the stop of feed delivery causes the concentration front to be at a standstill. In the production step, the concentration front moves to the top of bed. By contrasting with the pressurization step, the concentration front in the depressurization step moves to the bottom of bed and becomes smoother. When the purge stream rinses from another bed, the concentration front becomes even smoother in the bed.

The flat-box adsorbers replacing the cylindrical adsorbers

As shown in Table 5, the performance of the flat-box adsorbers with $h' = 14.049 \text{ J/K-m}^2\text{-s}$ was similar to that of the traditional cylindrical adsorbers at the same purge to feed ratio and product to feed ratio. But the flat-box adsorbers were better than the cylindrical adsorbers in the usage of packing space. When the heat transfer coefficient between neighboring adsorbers is $100 \text{ J/K-m}^2\text{-s}$, the performance unexpectedly was the worst result of three different design of h' for flat-box adsorbers. Heat transfer rate to neighboring flat-box adsorber is different for different h' , and at the end of purge

step the adsorber temperature profile becomes Run 3 > Run 2 > Run 1, shown in Figure 8. At the end of pressurization step the adsorber temperature profile becomes Run 1 \approx Run 2 > Run 3, shown in Figure 9. In other words, Run 1 and Run 2 have the similar adsorbed amount at the same time, shown in Figure 10 and Figure 11. After production step, higher heat transfer rate between neighboring adsorbers enables higher adsorbed amount of N₂. The desorbed oxygen amount in the production step for Run 1 is similar to that of Run 2. At the same time, feed ratio of Run 2 to Run 1 is close to the ratio of adsorbed nitrogen amount of Run 2 to Run 1. Consequently, the oxygen purity in product for Run 1 is higher than that of Run 2, shown in Table 6.

As the heat transfer coefficient between neighboring adsorbers increases from 14.049 to 1000 J/K-m²-s, the oxygen purity in product from air becomes better. The cause of this effect is that the adsorbed nitrogen amount at production step for Run 3 is more than that of Run 1, and the desorbed oxygen amount at production step for Run 3 is more than that of Run 1. Although the feed amount of Run 1 is less than that of Run 3, purity of Run 3 is still better than that of Run 1.

Effect of 1st & 3rd step time

The simulation results for various 1st & 3rd step time with three kinds of h' are presented in Tables 7-9. Figures 12-14 show the effect of 1st & 3rd step time with $h' = 14.049, 100, \text{ and } 1000 \text{ J/K-m}^2\text{-s}$. Both the feed flow rate and the product flow rate decrease with increasing 1st & 3rd step time. The reason is because the longer 1st & 3rd step time causes the smaller ratio of the production step time to cycle time. At $h' = 14.049 \text{ J/K-m}^2\text{-s}$, the purity slightly increases when 1st & 3rd step time increases. From Figures 15 and 16, the temperature difference between two adsorbers only slightly changes when 1st & 3rd step time changes from 40 s to 56s, the performance of PSA consequently is similar. When h' raises to 100 J/K-m²-s, the temperature of two adsorbers become close by increasing 1st & 3rd step time, shown in Figures 17-18. Thus the PSA separation becomes better when 1st & 3rd step time increases. As observed from Figures 19-20, the temperature of two adsorbers reach equilibrium around 36 s at $h' = 1000 \text{ J/K-m}^2\text{-s}$. For this reason, increasing 1st & 3rd step time higher than 36 s seems useless to heighten the purity.

Effect of 2nd & 4th step time

The results of the influence of 2nd & 4th step time are presented in Tables 10. The feed flow rate decrease with increasing 2nd & 4th step time, because in this range the raise of the amount of feed per cycle is smaller than that of cycle time, shown in Figure 21. Relatively, that in this range the raise of the amount of product per cycle is

bigger than that of cycle time results in product flow rate decreasing with increasing 2nd & 4th step time, shown in Figure 22. As observed from Figures 23, the purity decreases when 2nd & 4th step time increases. The cause is because workload of 5A zeolite become more as production step time increasing.

Effect of the bed length

Table 11 and Figure 24 show simulation results of varying the bed length. The feed flow rate increase with increasing bed length. This reason is that because as adsorbers become longer, more feed is needed to pressurize the adsorbers to reach the same pressure. The curve of the product flow rate versus bed length is nearly constant, because the stream of two ends of adsorbers is nearly identical to keep the same high bed pressure in the production step. As the adsorbers become longer, more 5A zeolite can separate gas mixtures. Thus the performance of PSA would be better for longer bed.

Effect of the adsorption pressure

At the same purge for feed ratio and product to feed ratio, the simulation results with reducing the adsorption pressure are shown in Table 12 and Figure 25. When the adsorption pressure is reduced from 4.26 atm to 3.26 atm, the purity decreases from 94.22% to 93.39% and the feed flow rate decreases to 76.80% of original. as adsorption pressure changes to 2.26 atm, the purity decreases to 88.58%. This result shows that the PSA process with adsorption pressure around 3.26 atm has the best performance.

5. Conclusions

The simulation program is verified by comparison of dual-bed process experimental results. After confirming the accuracy of the simulation program, the traditional cylindrical adsorbers were replaced by compact flat-box adsorbers. According to the comparison between the performance of cylindrical adsorbers and flat-box adsorbers, the flat-box adsorbers are on a par with the cylindrical adsorbers for the ability to separate gas mixtures. But the flat-box adsorbers have a superiority of better usage of packing space. For the flat-box adsorbers, as the feed pressure is reduced from 4.26 atm to 3.26 atm, the feed flow rate changes from 3.75 L/min to 2.88 L/min. A little price was paid: the oxygen purity in product is reduced from 94.22% to 93.39%, but less cost of electric power is used by pump.

Nonmenclature

- A : cross area of the packing bed [m^2]
 A_i, B_i : isotherm constants
 b_h : flat-box bed height [m]
 b_w : flat-box bed width [m]
 \bar{C}_p : heat capacity of gas mixtures [J/mole-K]
 \tilde{C}_p : heat capacity of component i [J/mole-K]
 \hat{C}_p : heat capacity of adsorbent [J/kg-K]
 c_v : valve flow coefficient
 D : cylindrical bed diameter [m]
 $D_{ax,i}$: axial dispersion coefficient [m^2/s]
 d_p : particle size of the adsorbent [m]
 H_i : adsorption heat of component i [J/mole]
 h : heat transfer coefficient between surrounding [J/K- m^2 -s]
 h' : heat transfer coefficient between neighboring adsorbers [J/K- m^2 -s]
 \bar{k} : average heat conduction coefficient [J/K-m-s]
 L : bed length [m]
 n_i : adsorbed amount of component i per unit volume of adsorbent [mole/m^3]
 n_i^* : equilibrium adsorbed amount of component i per unit volume of adsorbent [mole/m^3]
 P : pressure [atm]
 Q : flow rate [L/s @ STP]
 q : molar flow rate [mole/s]
 R : gas constant [m^3 -atm/mole-K]
 T : temperature [K]
 T_A : temperature of neighboring adsorber [K]
 T_∞ : room temperature [K]
 t : time [s]
 y_i : mole fraction of component i in gas phase

- z : axial coordinate, [m]
 ρ_s : particle density [kg/m³]
 ε : porosity, dimensionless

References

- Breck, D.W., *Zeolite Molecular Sieves*, Wiley Publishers, New York (1974)
- Boniface, H., *Separation of argon from air using zeolites*, Ph.D. thesis, University of New Brunswick, Fredericton (1983)
- Chou, C. T. and Huang, W. C. (1994) *Chemical Engineering Science*, 49(1), 75-84
- Farooq, S., Ruthven, D. M. and Boniface, H. A., (1989) *Chemical Engineering Science*, 44(12), 2809-2816.
- Huang W. J., Chen, C. Y. and Chou, C. T. (2006) *Journal of the Chinese Institute of Chemical Engineers*, 37(2), 149-157
- Verelat, H. and Baron, G. V. (1985) *Journal of Chemical Ecology*, 30(1), 66-70
- Zhou, L., Ouyang, X. F., Li, W., Li, S. N. and Zhou, Y. P. (2006) *Separation Science & Technology*, 41(2), 247-259.

Table 1 Characteristics of adsorbers

Bed length (L)	3.5000E-01 m*
Cylindrical bed diameter (D)	3.5000E-02 m*
flat-box bed height (b_h)	6.9358E-02 m
flat-box bed width (b_w)	1.3872E-02 m
Bed volume	3.3674E-01 L*
Porosity	4.0000E-01 *
Heat transfer coefficient (h)	3.1482E-04 J/K-m ² -s

*Farooq et al.(1989)

Table 2 Characteristics of adsorbent

Adsorbent	5A Zeolite
Particle density (ρ_s)	1.2020E+03 kg/m ³
Heat capacity of adsorbent (C_{ps})*	7.9000E+02 J/K-kg
Particle diameter (d_p) [§]	7.0700E-04 m

Parameters of the extended Langmuir isotherms of pure adsorbates

Oxygen

$$a_1^{\pounds} \quad 1.5510E-04 \text{ mole/g-(kgf/cm}^2\text{)}$$

$$b_1^{\pounds} \quad 3.3333E-02 \text{ (kgf/cm}^2\text{)}^{-1}$$

$$\text{Adsorption heat of Oxygen } (\Delta H_1)^{\pounds} \quad 1.3910E+04 \text{ J/mole}$$

Nitrogen

$$a_2^{\pounds} \quad 4.9498E-04 \text{ mole/g-(kgf/cm}^2\text{)}$$

$$b_2^{\pounds} \quad 1.7650E-01 \text{ (kgf/cm}^2\text{)}^{-1}$$

$$\text{Adsorption heat of Nitrogen } (\Delta H_2)^{\pounds} \quad 2.0420E+04 \text{ J/mole}$$

*Breck(1974)

§Farooq et al.(1989)

₤Boniface(1983)

ⓂVerelat and Baron(1985)

Table 3 Operating variables *

Feed composition	21% oxygen, 79% nitrogen
Room temperature	298.14 K
Feed temperature	298.14 K
Adsorption pressure	4.2600 atm
Blowdown pressure	1.0000 atm
Purge pressure	1.0700 atm
Feed flow rate	3.6664 L/min @ STP
Product flow rate	0.2188 L/min @ STP
Step time	48s, 32s, 48s, 32s

*Farooq et al.(1989)

Table 4 Experimental data and simulation results

	Experimental date *	Simulation results
Average feed flow rate [L/min @ STP]	3.67	3.69
Average vent flow rate [L/min @ STP]		2.52
Average waste flow rate [L/min @ STP]		0.95
Average product flow rate [L/min @ STP]	0.22	0.22
Purge to feed ratio [%]		16.46
Product to feed ratio [%]		5.93
Purity [%]	95.50	94.46
Recovery [%]	27.10	26.68

*Farooq et al.(1989)

Table 5 Simulation results of cylindrical adsorbers and flat-box adsorbers.

	Cylindrical adsorbers	Flat-box adsorbers		
		Run 1	Run 2	Run 3
		$h' = 14.049$ J/K-m ² -s	$h' = 100$ J/K-m ² -s	$h' = 1000$ J/K-m ² -s
Average feed flow rate [L/min @ STP]	3.69	3.75	4.11	4.68
Average vent flow rate [L/min @ STP]	2.52	2.54	2.73	3.14
Average waste flow rate [L/min @ STP]	0.95	0.98	1.13	1.26
Average product flow rate [L/min @ STP]	0.22	0.22	0.24	0.28
Purge to feed ratio [%]	16.46	16.46	16.46	16.46
Product to feed ratio [%]	5.93	5.93	5.93	5.93
Purity [%]	94.46	94.22	93.18	95.13
Recovery [%]	26.68	26.60	26.31	26.87

Table 6 The effect of heat transfer coefficient between neighboring adsorbers of flat-box adsorbers in the production step

	Value			Ratio with respect to Run1		
	Run 1	Run 2	Run 3	Run 1	Run 2	Run 3
The oxygen amount of desorption [L at STP]	0.6005	0.6192	0.7314	-	103.12%	121.81%
The nitrogen amount of adsorption [L at STP]	1.0587	1.2498	1.4512	-	118.06%	137.08%
The change amount of oxygen on gas phase	-0.0998	-0.1041	-0.1176	-	104.32%	117.80%
The change amount of nitrogen on gas phase	0.0945	0.1012	0.1138	-	107.15%	120.41%
The amount of feed [L at STP]	1.5462	1.8273	2.0796	-	118.18%	134.50%
Purity	94.22%	93.18%	95.13%			

Table 7 The effect of 1st & 3rd step time with $h' = 14.049 \text{ J/K-m}^2\text{-s}$

1st & 3rd step time [s]	40	44	48	52	56
Cycle time [s]	144	152	160	168	176
Average feed flow rate [L/min @ STP]	4.15	3.94	3.75	3.57	3.41
Average vent flow rate [L/min @ STP]	2.81	2.67	2.54	2.42	2.31
Average waste flow rate [L/min @ STP]	1.09	1.04	0.98	0.94	0.89
Average product flow rate [L/min @ STP]	0.25	0.23	0.22	0.21	0.20
Purge to feed ratio [%]	16.50	16.48	16.46	16.45	16.43
Product to feed ratio [%]	5.94	5.94	5.93	5.92	5.91
Purity [%]	94.19	94.21	94.22	94.22	94.23
Recovery [%]	26.66	26.63	26.60	26.56	26.53

Table 8 The effect of 1st & 3rd step time with $h' = 100 \text{ J/K-m}^2\text{-s}$

1st & 3rd step time [s]	40	44	48	52	56
Cycle time [s]	144	152	160	168	176
Average feed flow rate [L/min @ STP]	4.53	4.31	4.11	3.93	3.77
Average vent flow rate [L/min @ STP]	2.99	2.85	2.73	2.62	2.52
Average waste flow rate [L/min @ STP]	1.26	1.19	1.13	1.08	1.03
Average product flow rate [L/min @ STP]	0.28	0.26	0.24	0.23	0.22
Purge to feed ratio [%]	16.51	16.47	16.46	16.46	16.45
Product to feed ratio [%]	6.09	6.01	5.93	5.85	5.77
Purity [%]	92.26	92.82	93.18	93.47	93.73
Recovery [%]	26.74	26.57	26.31	26.03	25.75

Table 9 The effect of 1st & 3rd step time with $h' = 1000 \text{ J/K-m}^2\text{-s}$

1st & 3rd step time [s]	40	44	48	52	56
Cycle time [s]	144	152	160	168	176
Average feed flow rate [L/min @ STP]	5.20	4.93	4.68	4.46	4.26
Average vent flow rate [L/min @ STP]	3.49	3.30	3.14	2.99	2.86
Average waste flow rate [L/min @ STP]	1.40	1.32	1.26	1.20	1.14
Average product flow rate [L/min @ STP]	0.31	0.29	0.28	0.26	0.25
Purge to feed ratio [%]	16.47	16.47	16.46	16.46	16.45
Product to feed ratio [%]	5.94	5.94	5.93	5.93	5.93
Purity [%]	95.10	95.11	95.13	95.14	95.16
Recovery [%]	26.92	26.88	26.87	26.85	26.85

Table 10 The effect of 2nd & 4th step time with $h' = 14.049 \text{ J/K-m}^2\text{-s}$

2nd & 4th step time [s]	26	29	32	35	38
Cycle time [s]	148	154	160	166	172
Average feed flow rate [L/min @ STP]	3.81	3.78	3.75	3.71	3.68
Amount of feed [L/cycle @ STP]	9.41	9.70	9.99	10.26	10.54
Average vent flow rate [L/min @ STP]	2.77	2.65	2.54	2.44	2.34
Average waste flow rate [L/min @ STP]	0.86	0.92	0.98	1.04	1.09
Average product flow rate [L/min @ STP]	0.19	0.21	0.22	0.24	0.25
Amount of product [L/cycle @ STP]	0.46	0.53	0.59	0.65	0.71
Purge to feed ratio [%]	14.39	15.45	16.46	17.49	18.52
Product to feed ratio [%]	4.92	5.44	5.93	6.34	6.69
Purity [%]	96.04	95.17	94.22	92.58	90.93
Recovery [%]	22.51	24.66	26.60	27.97	28.98

Table 11 The effect of bed length with $h' = 14.049 \text{ J/K-m}^2\text{-s}$

Bed length [m]	0.29	0.32	0.35	0.38	0.41
Bed volume [L]	0.2790	0.3079	0.3367	0.3656	0.3945
Average feed flow rate [L/min @ STP]	3.29	3.52	3.75	3.97	4.19
Average vent flow rate [L/min @ STP]	2.08	2.31	2.54	2.77	2.99
Average waste flow rate [L/min @ STP]	0.98	0.98	0.98	0.98	0.98
Average product flow rate [L/min @ STP]	0.22	0.22	0.22	0.22	0.22
Purge to feed ratio [%]	18.83	17.53	16.46	15.57	14.80
Product to feed ratio [%]	6.69	6.32	5.93	5.55	5.20
Purity [%]	90.49	92.65	94.22	95.11	95.63
Recovery [%]	28.82	27.87	26.60	25.13	23.68

Table 12 The effect of adsorption pressure with $h' = 14.049 \text{ J/K}\cdot\text{m}^2\cdot\text{s}$

Adsorption pressure [atm]	2.26	3.26	3.56	3.86	4.06	4.26
Average feed flow rate [L/min @ STP]	1.79	2.88	3.16	3.42	3.58	3.75
Average vent flow rate [L/min @ STP]	1.20	1.93	2.13	2.31	2.43	2.54
Average waste flow rate [L/min @ STP]	0.49	0.77	0.84	0.91	0.95	0.98
Average product flow rate [L/min @ STP]	0.11	0.17	0.19	0.20	0.21	0.22
Purge to feed ratio [%]	16.46	16.46	16.46	16.46	16.47	16.46
Product to feed ratio [%]	5.93	5.93	5.93	5.93	5.93	5.93
Purity [%]	88.58	93.39	93.73	93.93	93.97	94.22
Recovery [%]	25.02	26.36	26.46	26.54	26.52	26.60

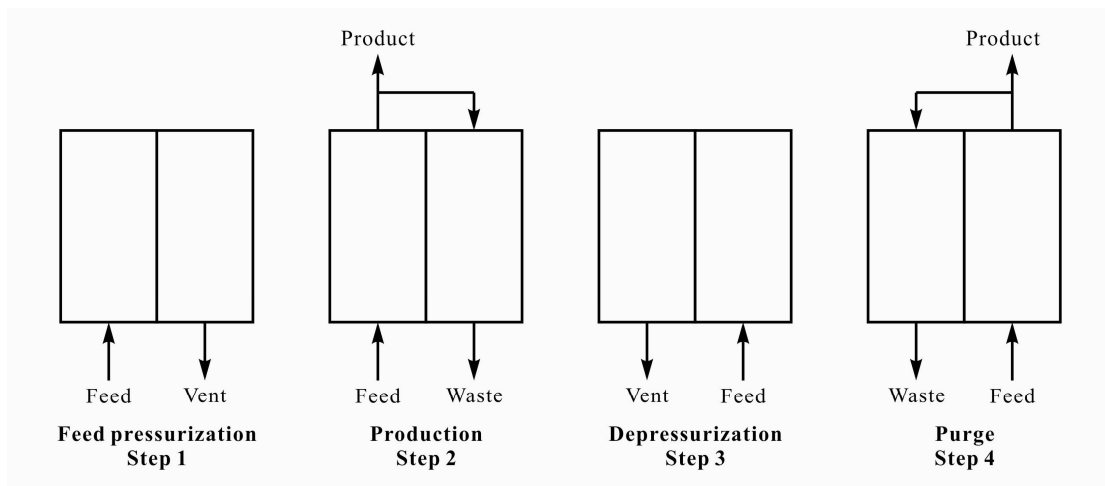


Figure 1 Skarstrom cycle

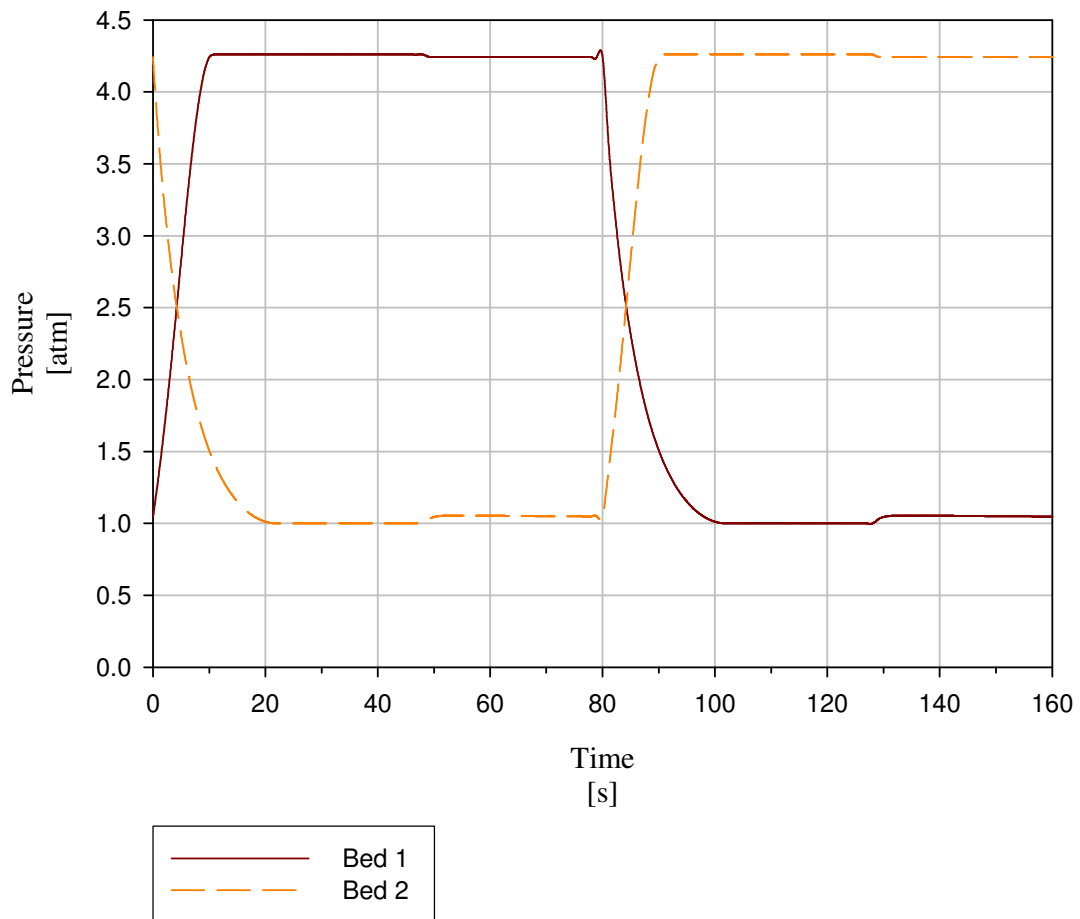


Figure 2 The change of pressure with time

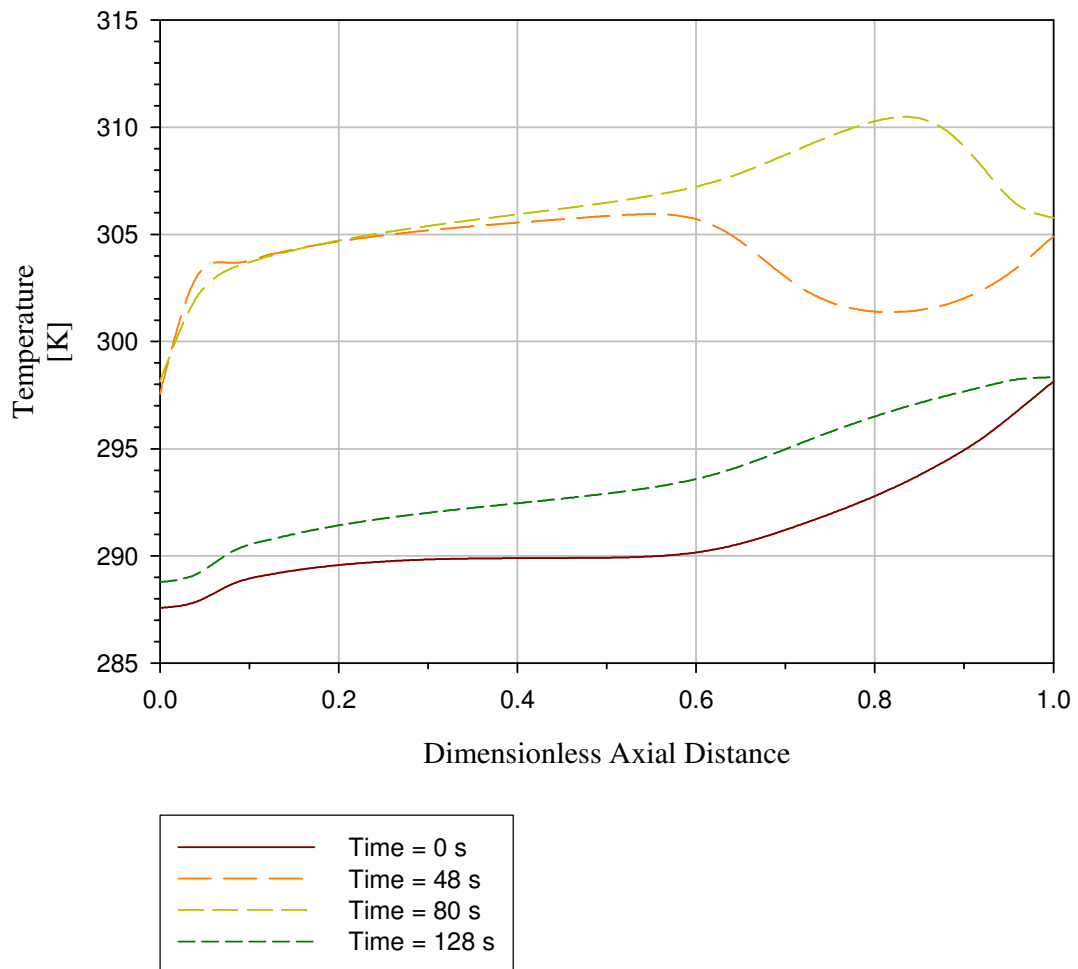


Figure 3 Temperature profile

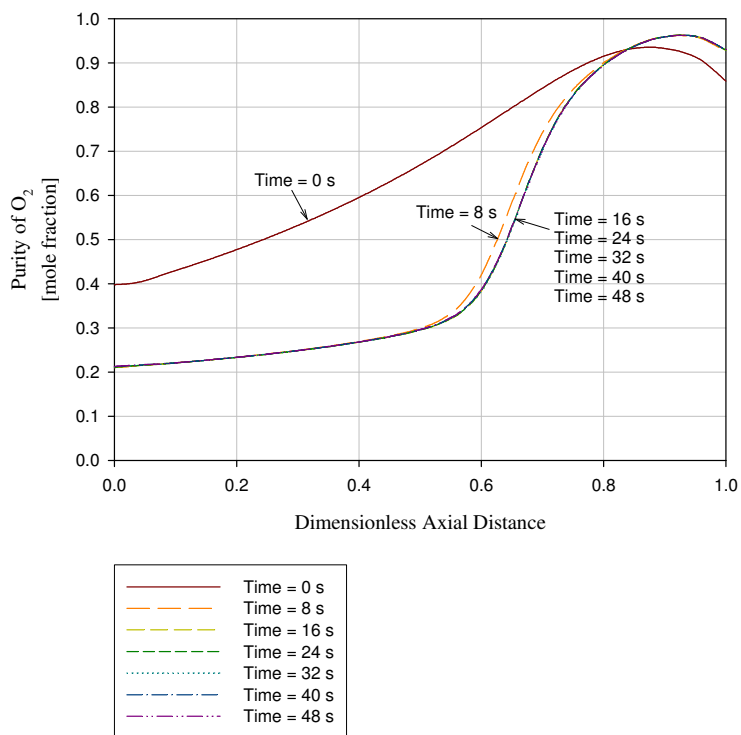


Figure 4 Purity of O₂ profile in the pressurization step

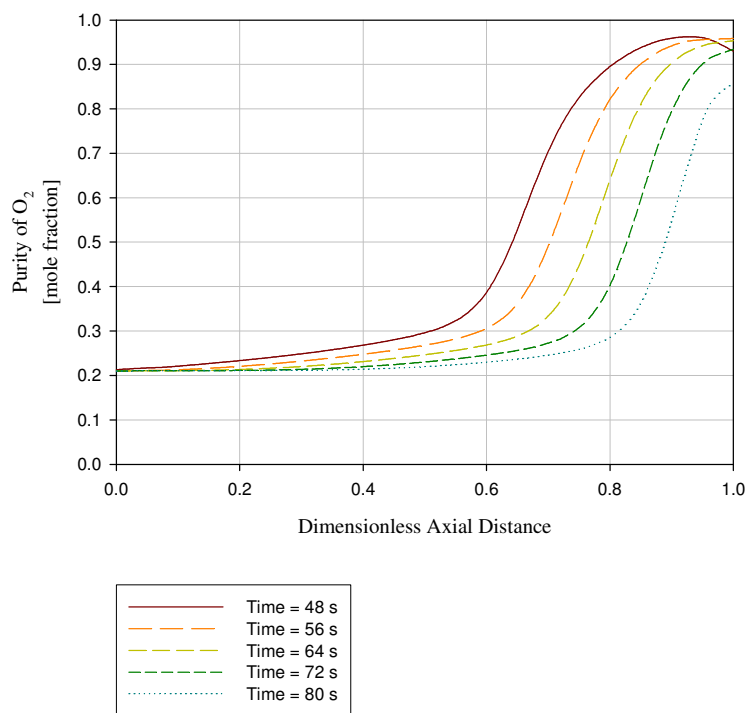


Figure 5 Purity of O₂ profile in the production step

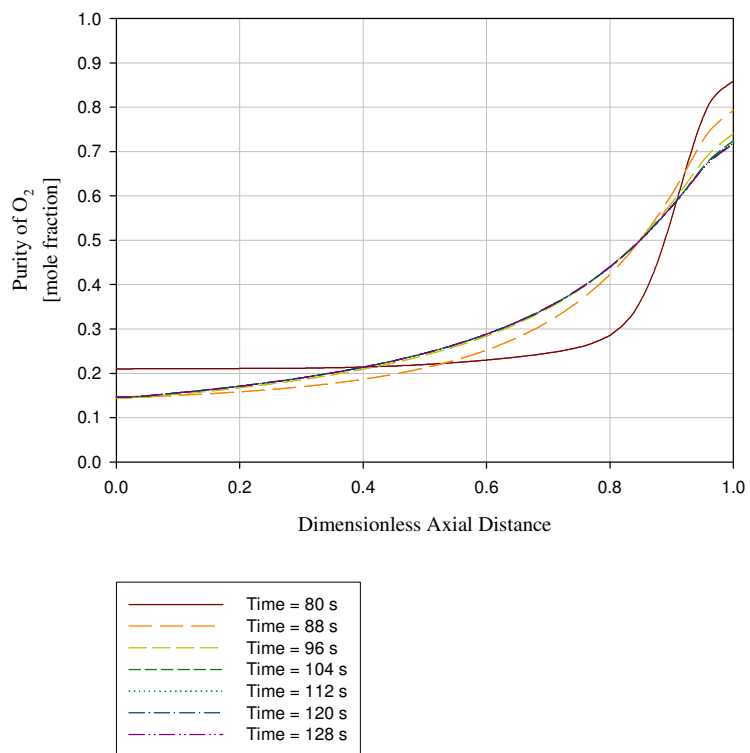


Figure 6 Purity of O₂ profile in the depressurization step

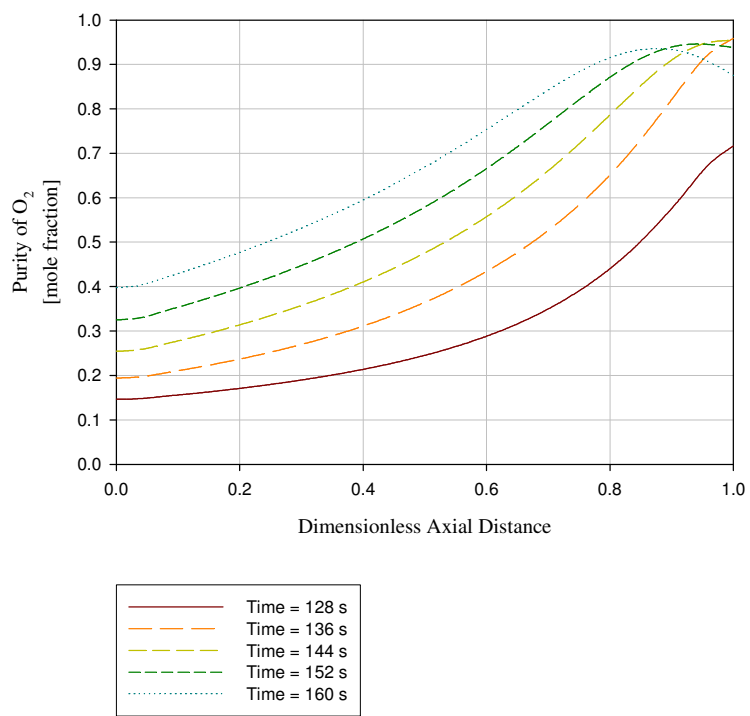


Figure 7 Purity of O₂ profile in the purge step

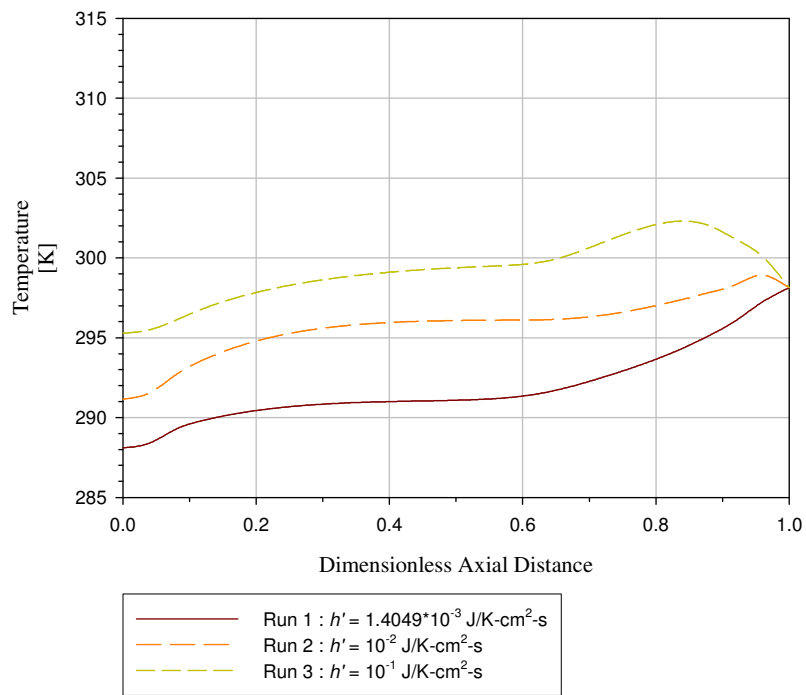


Figure 8 Temperature profile at time = 0 s

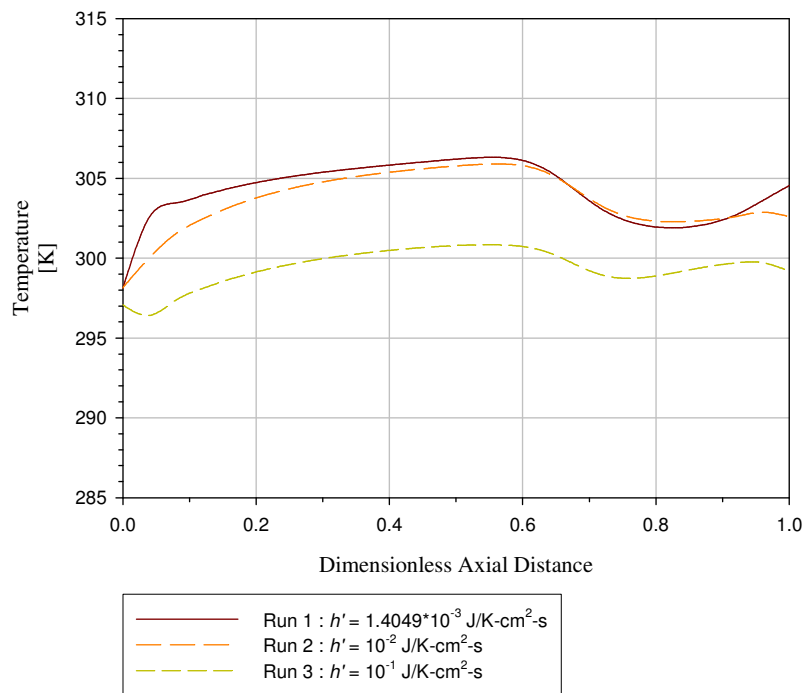


Figure 9 Temperature profile at time = 48 s

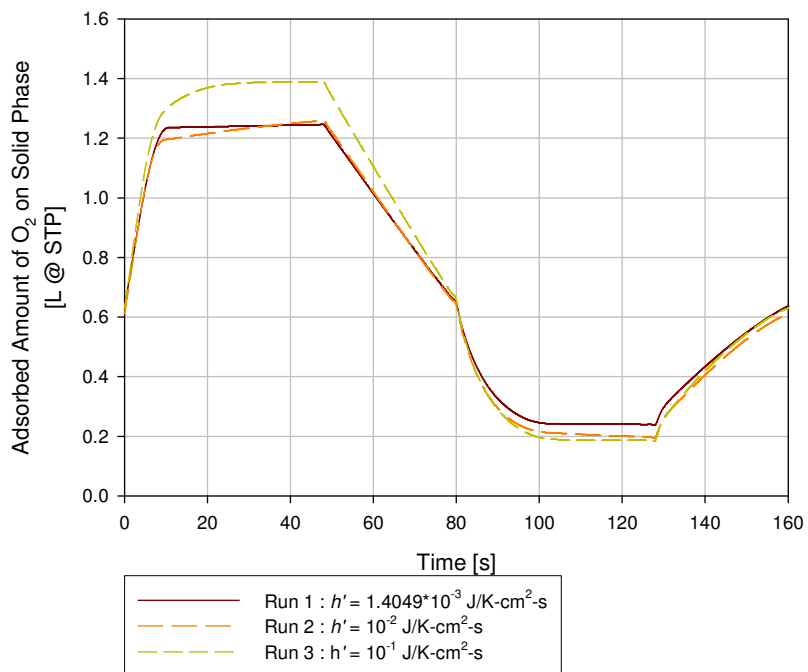


Figure 10 Change of adsorbed amount of O₂ on solid phase with time

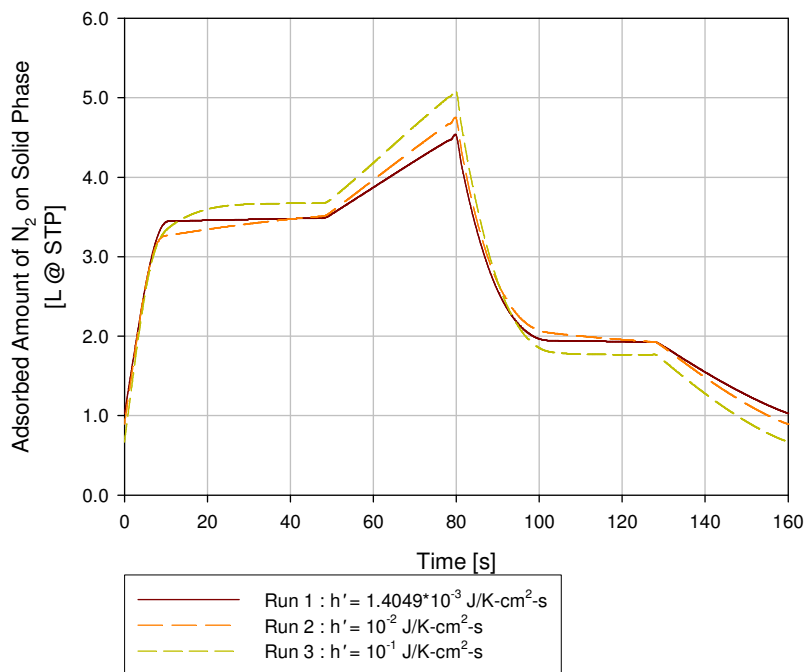


Figure 11 Change of adsorbed amount of N₂ on solid phase with time

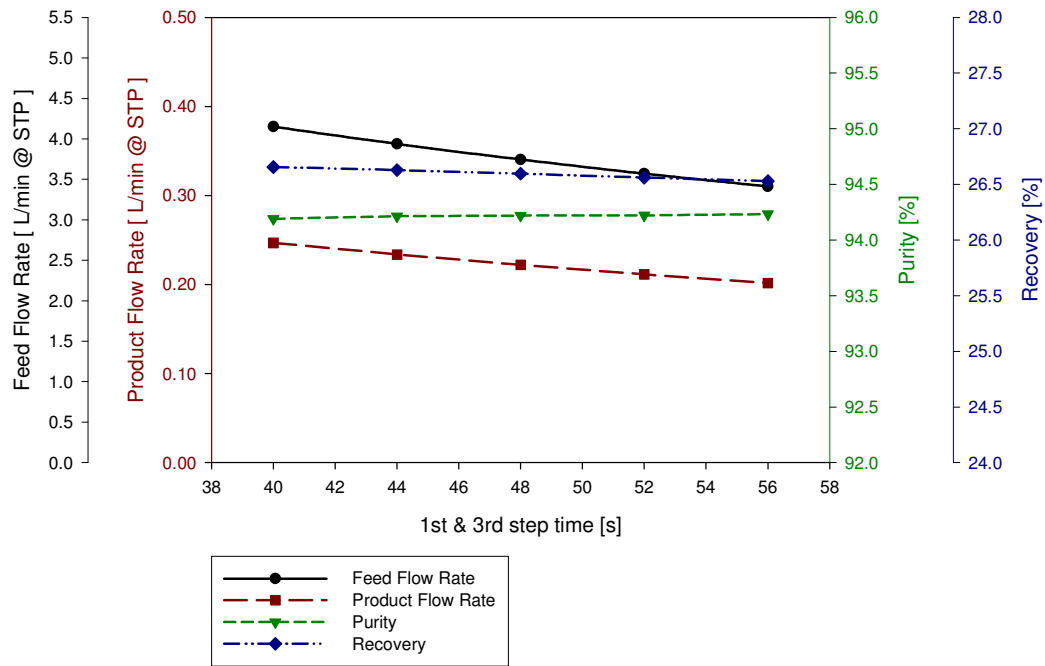


Figure 12 The effect of 1st & 3rd step time on feed flow rate, product flow rate, purity, and recovery with $h' = 14.049 \text{ J/K-m}^2\text{-s}$

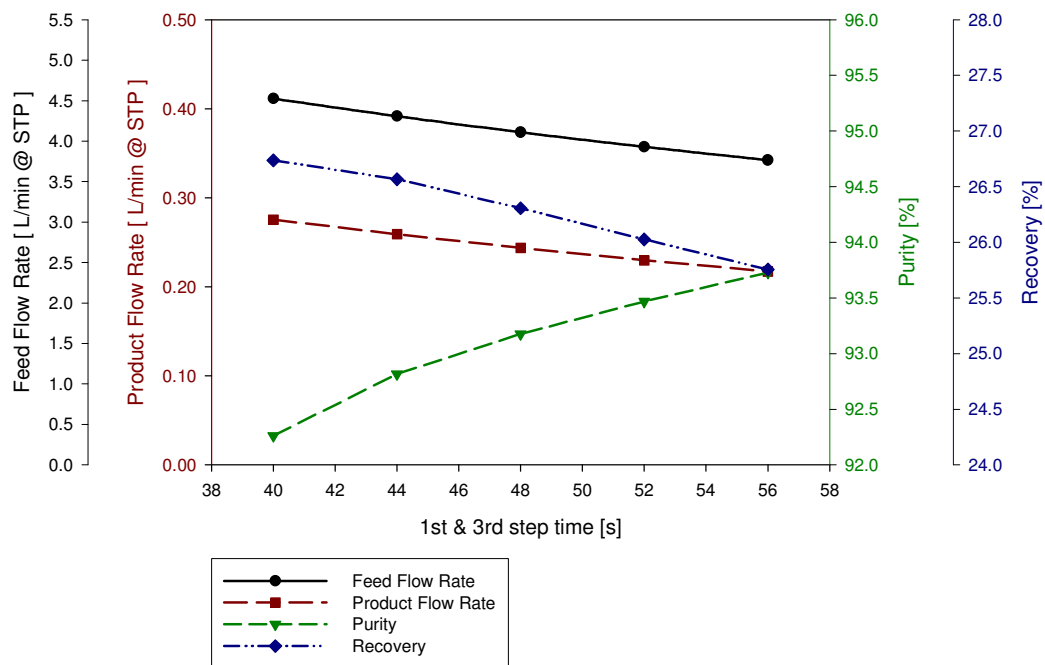


Figure 13 The effect of 1st & 3rd step time on feed flow rate, product flow rate, purity, and recovery with $h' = 100 \text{ J/K-m}^2\text{-s}$

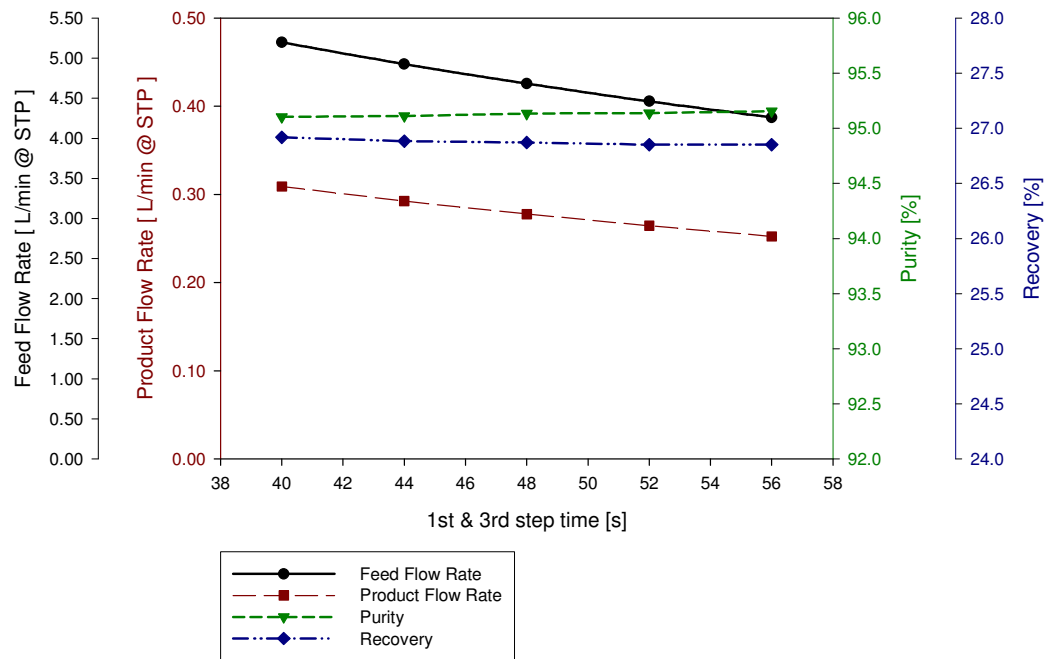


Figure 14 The effect of 1st & 3rd step time on feed flow rate, product flow rate, purity, and recovery with $h' = 1000 \text{ J/K-m}^2\text{-s}$

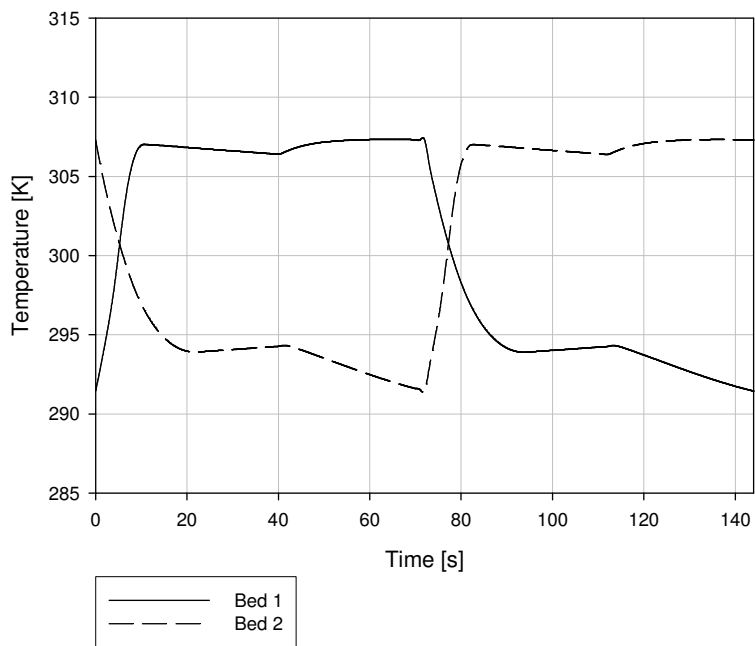


Figure 15 The change of temperatur with time at dimensionless axial distance = 0.6 with $h' = 14.049 \text{ J/K-m}^2\text{-s}$ and 1st & 3rd step time = 40 s

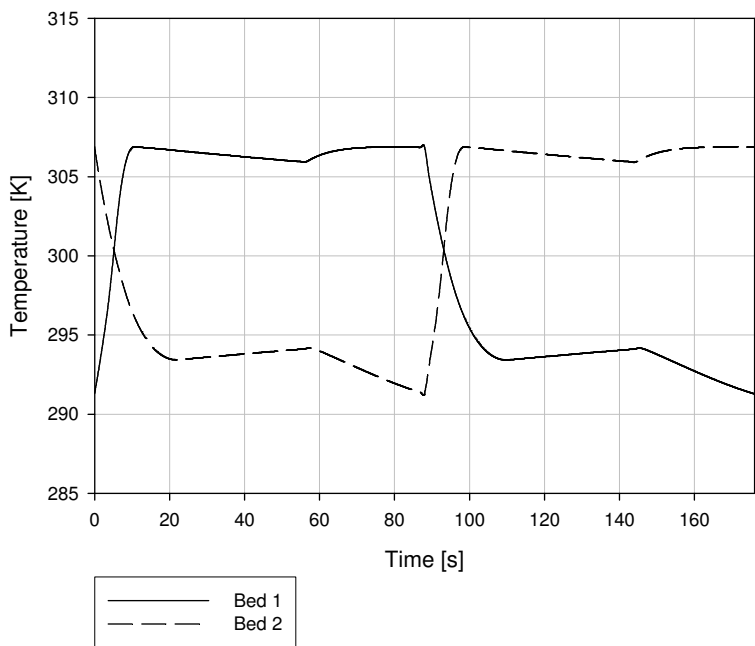


Figure 16 The change of temperatur with time at dimensionless axial distance = 0.6 with $h' = 14.049 \text{ J/K-m}^2\text{-s}$ and 1st & 3rd step time = 56 s

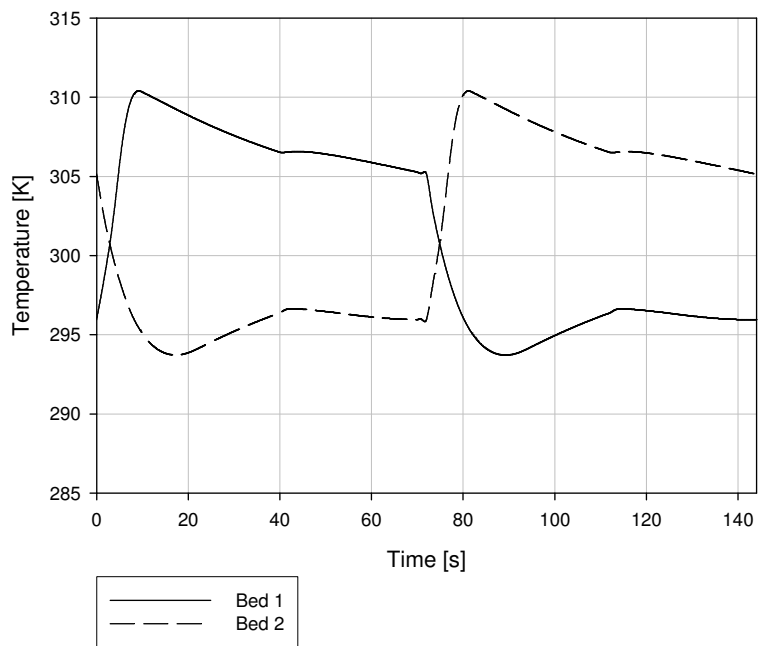


Figure 17 The change of temperatur with time at dimensionless axial distance = 0.6 with $h' = 100 \text{ J/K-m}^2\text{-s}$ and 1st & 3rd step time = 40 s

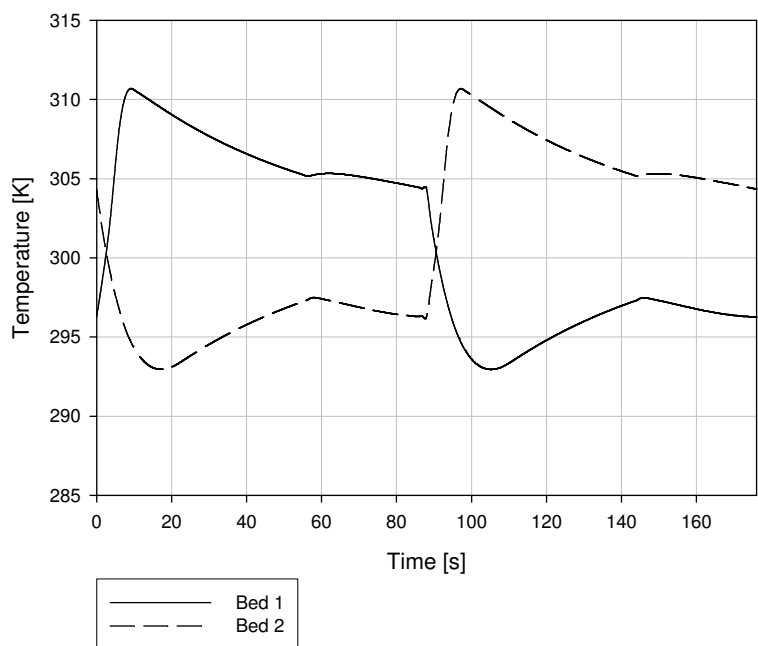


Figure 18 The change of temperatur with time at dimensionless axial distance = 0.6 with $h' = 100 \text{ J/K-m}^2\text{-s}$ and 1st & 3rd step time = 56 s

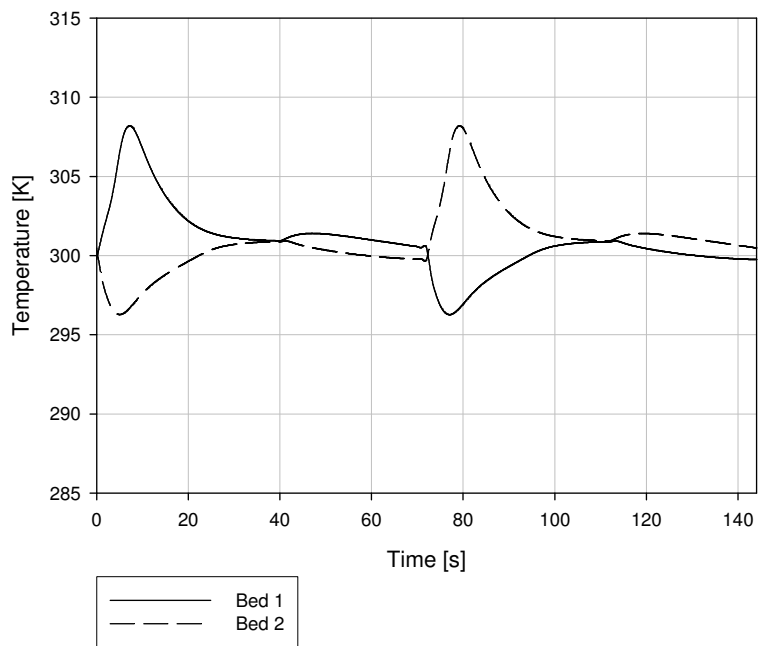


Figure 19 The change of temperatur with time at dimensionless axial distance = 0.6 with $h' = 1000 \text{ J/K-m}^2\text{-s}$ and 1st & 3rd step time = 40 s

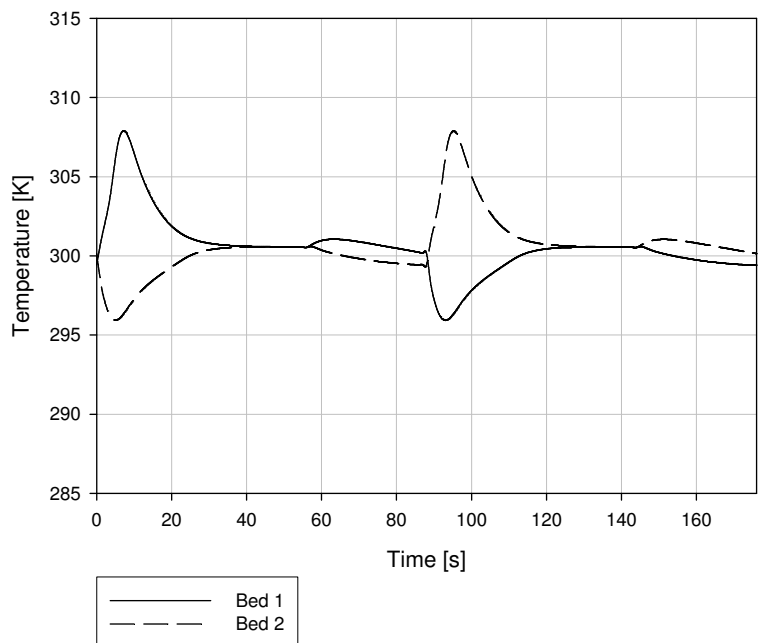


Figure 20 The change of temperatur with time at dimensionless axial distance = 0.6 with $h' = 1000 \text{ J/K-m}^2\text{-s}$ and 1st & 3rd step time = 56 s

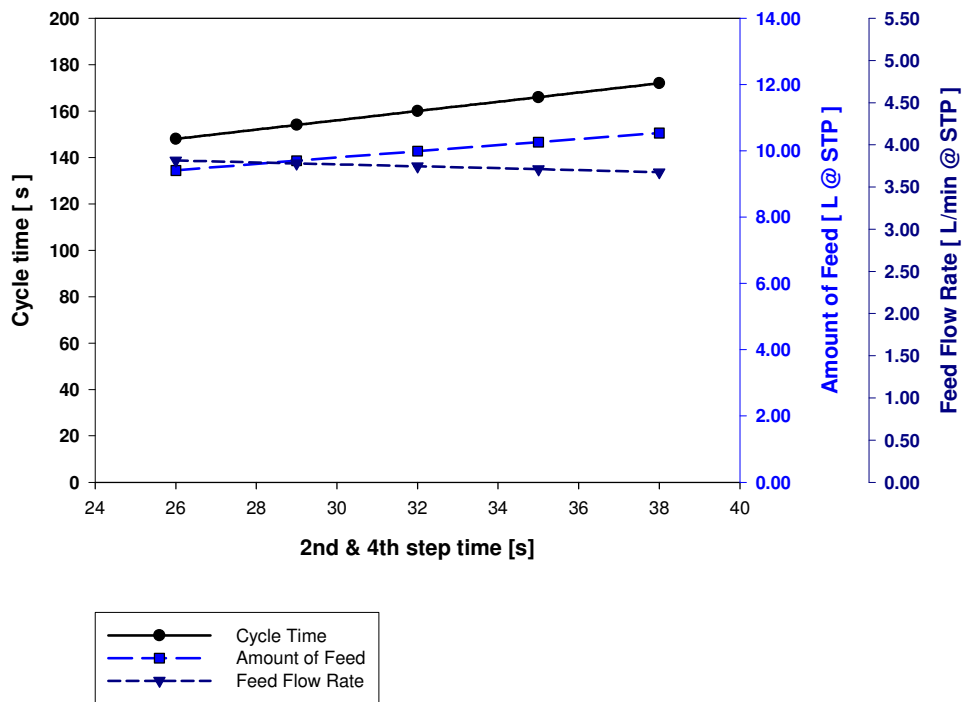


Figure 21 The effect of 2nd & 4th step time on feed cycle time, amount of feed, and feed flow rate with $h' = 14.049 \text{ J/K-m}^2\text{-s}$

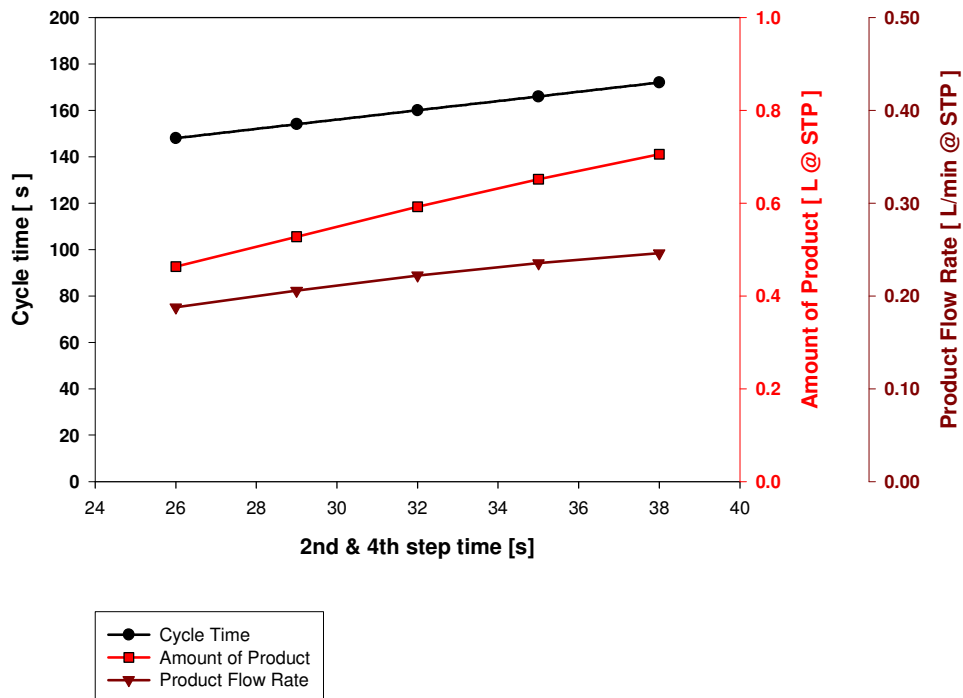


Figure 22 The effect of 2nd & 4th step time on feed cycle time, amount of product, and product flow rate with $h' = 14.049 \text{ J/K-m}^2\text{-s}$

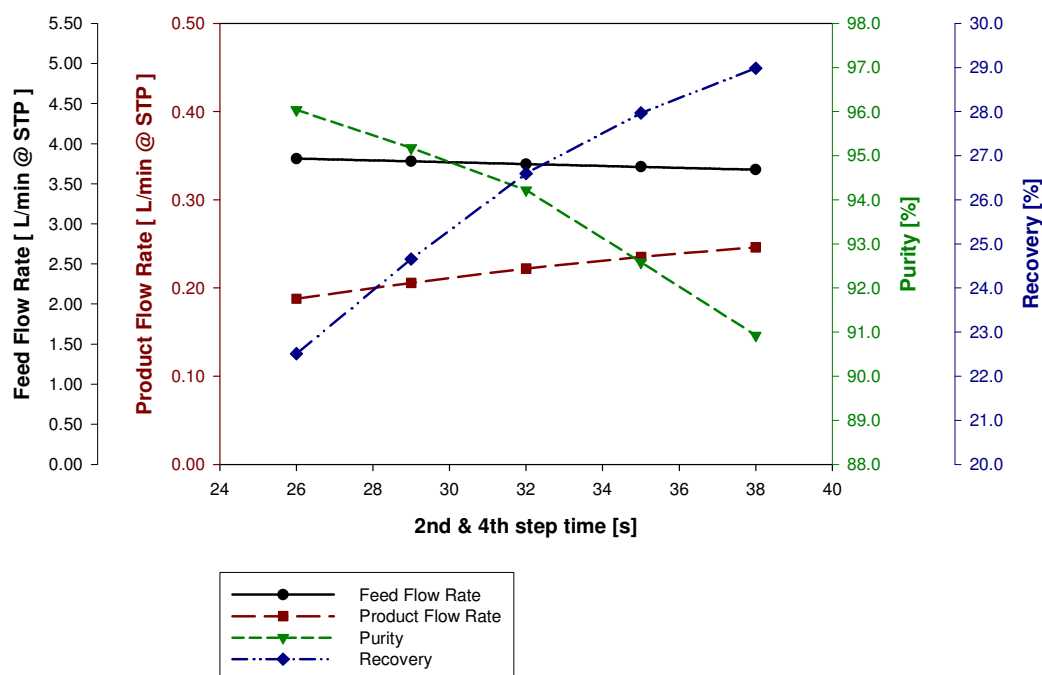


Figure 23 The effect of 2nd & 4th step time on feed flow rate, product flow rate, purity, and recovery with $h' = 14.049 \text{ J/K-m}^2\text{-s}$

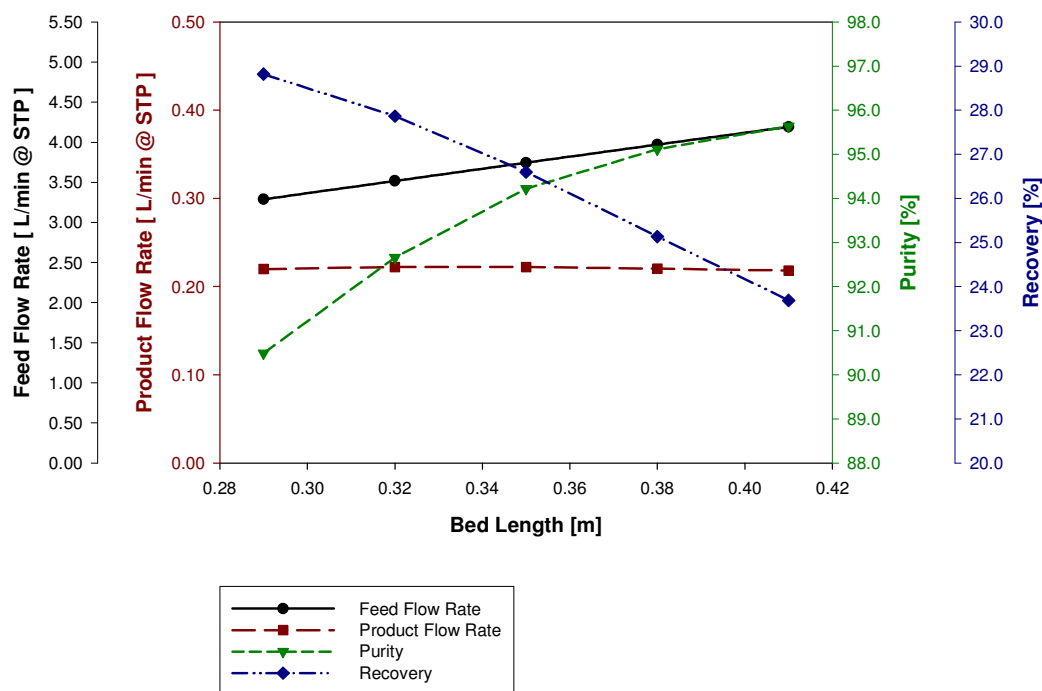


Figure 24 The effect of bed length on feed flow rate, product flow rate, purity, and recovery with $h' = 14.049 \text{ J/K-m}^2\text{-s}$

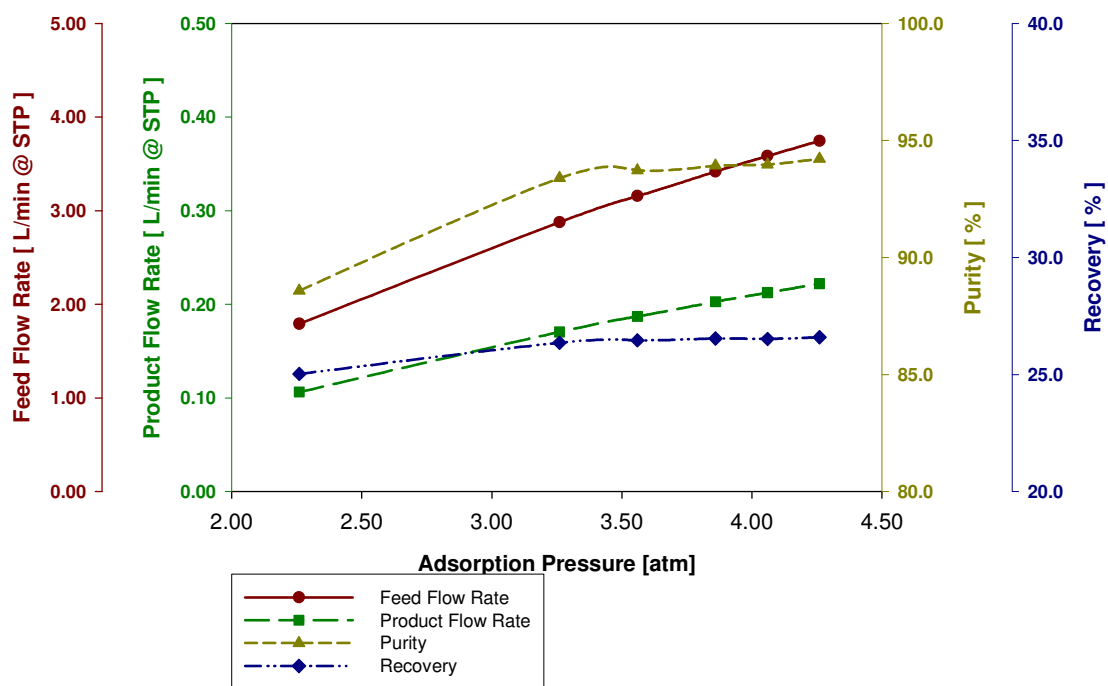


Figure 25 The effect of adsorption pressure on feed flow rate, product flow rate, purity, and recovery with $h' = 14.049 \text{ J/K-m}^2\text{-s}$